Evidence of pockmarks and seafloor gas venting in the northwestern Arabian Sea

Check for updates

Ahmed Abdelmaksoud [1] ✉, Aisha H. Al-Suwaidi[1], Moamen Ali [1], Azeem Shah[1], Sara S. Almehairbi[2], Lamia M. Al Ali[2] & Mohammed Y. Ali [1]

Marine gas seeps are common along tectonically active margins, but they have not been previously observed along the Arabian continental margin. Here we present evidence of gas escape structures, pockmarks, and active gas seeps in the Gulf of Oman. Multibeam bathymetry, water column backscatter and physical parameters, and two-dimensional seismic reflection data were used to map active seafloor seeps and pockmarks. Circular and crescent-shaped pockmarks and complex pockmark strings were identified. These features are confined to regions shoreward of the shelf break. Thirty-five active gas bubble trains were observed, mostly not coincident with the mapped pockmarks. With progressive gas release, the gas seeps are anticipated to lead to development of pockmarks over time. Bright spots on the seismic data indicate shallow subsurface gas accumulation alongside normal fault and fracture conduits, strongly correlated to the presence of pockmarks. These findings suggest an important carbon flux into the Arabian Sea and atmosphere.

Seafloor pockmarks are crater-like depressions that occur wherever fluid or gas flow is focused in low-permeability, fine-grained sediments[1,2]. The most common mechanism for pockmark formation is fluid or gas escape from marine sediments. The escaping fluids may be thermogenic gas[3], biogenic gas[4,5] (e.g., methane, hydrogen sulfide, or dissociated gas hydrates[6–9]), interstitial water expelled during compaction[10,11], or flowing groundwater[12–14]. Pockmark formation depends on, among other factors, seafloor sediment lithology and/or oceanographic setting[3,15–18]. Pockmarks vary in size, shape, and distribution[19–22]. As seafloor obstacles or irregular surfaces, pockmarks can be reshaped through scouring or erosion by bottom currents and associated turbulence, especially in hydrodynamically energetic oceanographic settings. The progressive erosion of these features may result in depressions up to hundreds of meters in length and tens of meters in depth[18,23–29].

The eastern offshore region of the United Arab Emirates (UAE, Fig. 1) within the Gulf of Oman is called the Fujairah basin[30]. This basin is bordered to the south by the Sohar basin, and by the Makran subduction zone and Minab-Zendan-Palami strike-slip system to the east and northeast[31–34]. It is bounded to the west by a major ~40–45° east-dipping major normal fault representing the eastern edge of the Semail ophiolite[35]. The Fujairah and Sohar basins lie adjacent to the northeastern margin of the Arabian Plate, along the eastern flank of the Oman-UAE mountains. The origin of these basins is traced back to the Late Cretaceous due to the Semail ophiolite obduction and the resultant gravitational collapsing along the eastern flank of the mountains[35–39]. The Semail ophiolite emplacement flexed down a previously rifted continental margin, hence contributing to the subsidence of flanking sedimentary basins, represented by the Fujairah and Sohar basins to the east and the Aruma basin to the west of the mountain belt[35,36,39–42]. The northeastern margin of the Arabian Plate is covered by ~10 km of Late Cretaceous to Quaternary sediments[35,36,39]. The Pleistocene-Holocene succession reflects a shallow marine shelf condition. It consists of limestone with calcareous claystone and siltstone[30]. The Pliocene succession reflects the outer shelf of shallow marine deltaic conditions. It comprises calcareous claystone, with calcareous limestone, siltstones, minor dolomites, and occasional igneous rock fragments[30]. The Miocene sequence was deposited in shallow marine to upper bathyal environments and consists of calcareous claystone with shale, silt, and conglomerates (including igneous clasts)[30]. The Oligocene sequence was deposited mainly in shallow marine conditions with a slight outer shelf influence. It consists of claystone with sand and occasional siltstones, marls, and minor conglomerates. The shallow to open-marine Eocene section comprises limestones, calcareous claystones, minor conglomerates, sands, silts, marls, and shales. The open-marine Paleocene sequence consists of limestone and calcareous claystone. The Upper Cretaceous sequence mainly comprises shales[30]. Radiocarbon dating of two core samples from the Strait of Hormuz and the Gulf of Oman indicated that the surface sediments in this area have an age range of ~14,000 years (directly to the south of the Strait of Hormuz) to 30,000 years (deep water of the Gulf of Oman)[43].

The Arabian/Persian Gulf is known for the occurrence of gas venting from the seafloor[3,44–46]. However, similar vents have not been reported in the

[1]Department of Earth Sciences, Khalifa University of Science and Technology, Abu Dhabi, UAE. [2]Environment Agency – Abu Dhabi, Abu Dhabi, UAE. ✉e-mail: ahmed.osman@ku.ac.ae

Fig. 1 | Map of the seafloor bathymetry of the eastern offshore of the UAE. The map covers the continental shelf, shelf break, slope base, and locating the newly discovered gas seeps (cyan circles). The yellow circles locate the water column physical parameters profiles with their numbers, whereas the gray lines refer to the seismic reflection profiles. Inset: the eastern Arabian continental margin; the light green area refers to the location of the acquired datasets. BONF Batinah Onshore Normal Fault, BOFNF Batinah Offshore Normal Fault, MuP Musandam Peninsula.
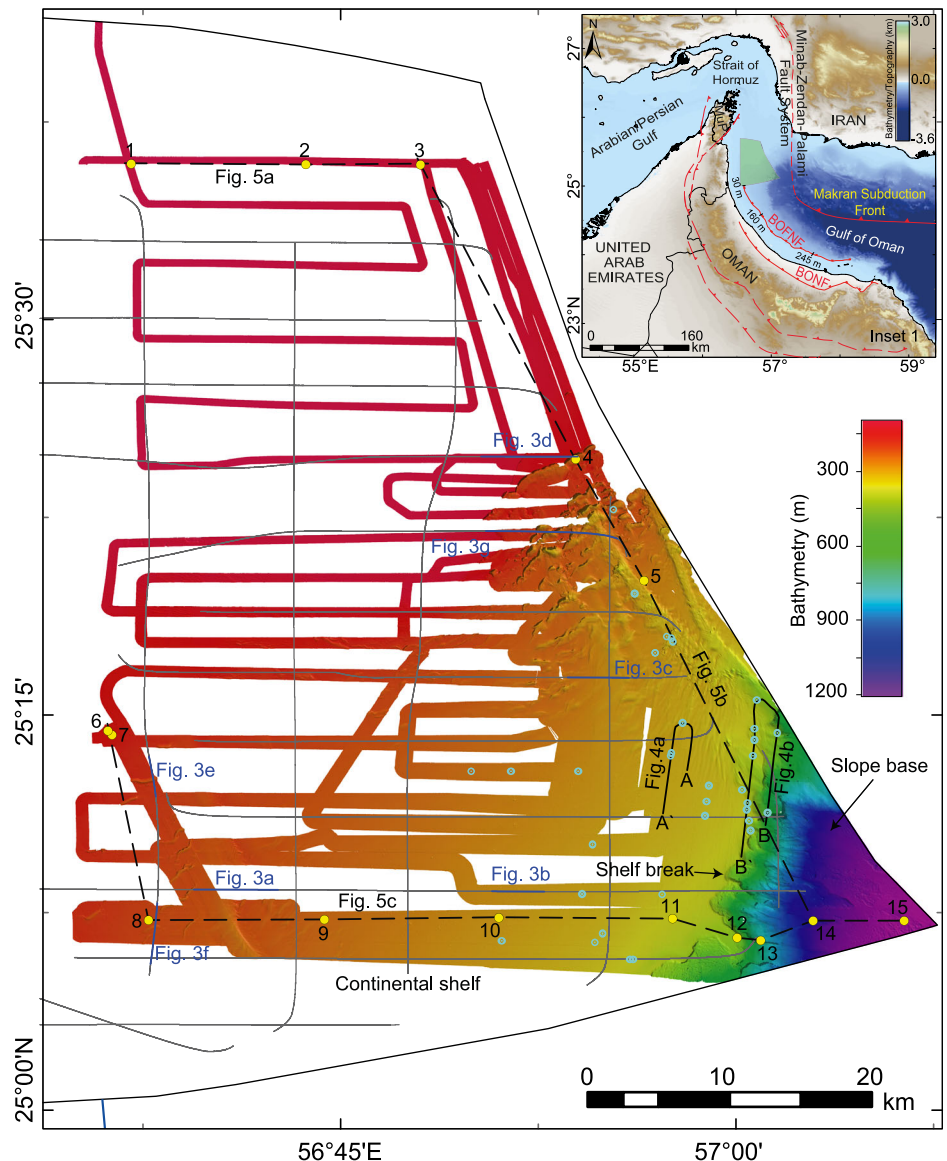
northwestern margin of the Arabian Sea (the eastern UAE-Oman continental margin of the Gulf of Oman). This area forms the northernmost extent of the Arabian Sea Oxygen Minimum Zone (OMZ), generally considered an area of increased carbon flux to the atmosphere[47,48]. Most studies of the Arabian Sea OMZ lack data in the northwestern-most waters, and as such, satellite-derived and modeled greenhouse gas flux calculations may not accurately estimate these fluxes for the Gulf of Oman[49,50]. The absence of reported gas seeps along this margin may be attributable to the limited geophysical surveying conducted in the northern Gulf of Oman. Here, we present geophysical data showing a giant pockmark field and the first evidence of gas escape, to the best of our knowledge, from the seafloor along this continental margin, using high-resolution multibeam bathymetry and wideband echosounding data, as well as profiles of the physical parameters (PPP) of the water column (e.g., salinity, temperature, and beam attenuation), integrated with two-dimensional (2D) seismic reflection data.

Results

Multibeam bathymetry observations

The multibeam bathymetry data covers an area of 1097 km² of the northeastern Arabian continental margin along the east coast of the UAE, from the shelf area passing through the shelf break and continental slope to the base of the slope (Fig. 1). The multibeam bathymetry indicates that the

seafloor depth ranges from 85 m below sea level in the northwestern sector to 1210 m in the southeastern sector (Fig. 1). We identified three types of pockmarks across the margin, namely circular, isolated crescent-shaped, and pockmark strings. A total of 1013 circular pockmarks were identified across the bathymetry dataset. These circular pockmarks occur at depths ranging from 104 to 493 m (Fig. 2a, b). We observed two clusters of circular pockmarks in the Gulf of Oman. The pockmarks of the first cluster occur at depths of 104–333 m and are symmetric in shape with diameters of 25–120 m. The pockmarks are 1.5–12 m deep relative to the surrounding bathymetry (Fig. 2b), and their rims have gentle slope gradients of 3–15°. The second cluster of circular pockmarks occurs near the shelf break (380–493 m depth). These pockmarks have a similar diameter to those in shallower water but are 10–20 m deeper than the surrounding seafloor and have slopes up to 45°. A total of 67 isolated crescent-shaped pockmarks and 73 areas with complex pockmark strings (connected crescent-shaped pockmarks) were identified at water depths of 130–235 m. The isolated crescent-shaped pockmarks have steep N-NW walls (average slope of 30°) and gentle S-SE ends (average slope of 11°) (Fig. 2c, d). The isolated crescent-shaped pockmarks are 90–500 m long and 100–300 m wide. Comparatively, the pockmark strings have lengths of up to 9000 m in the NE sector at depths of 125–270 m with widths of 150–600 m. The pockmark strings exhibit a similar slope pattern to the isolated crescent-shaped pockmarks, with very
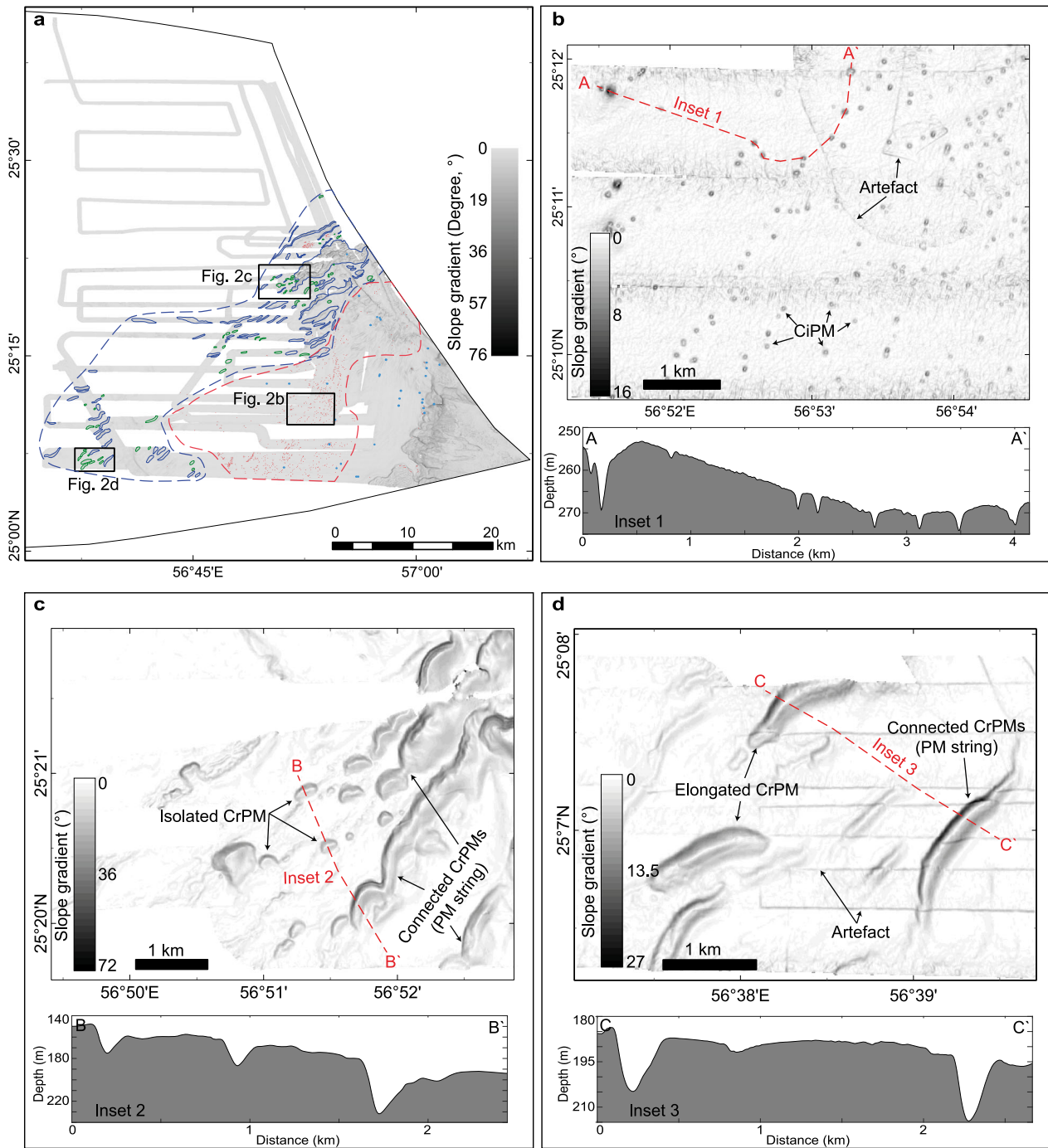
Fig. 2 | Slope gradient maps of the eastern offshore of the UAE. a A slope gradient map derived from the multibeam bathymetry, showing the locations of **b–d**. The light blue circles represent the discovered gas seeps, the red dots refer to the circular pockmarks (CiPM), and the solid green and blue polygons refer to the crescent-shaped pockmarks (CrPM) and complex pockmark strings (PM strings), respectively. The dashed blue and red polygons represent areas containing most of the complex-shaped pockmarks and the simple circular pockmarks, respectively. **b–d** highlight the different pockmark geometries with inset 1–3 as bathymetric profiles across these pockmarks.

steep northern edges (up to 55°) and relatively less steep southern boundaries with 20° slopes typically (Fig. 2c, d).

Seismic and water column backscatter observations

The 2D seismic reflection data comprises 20 profiles, covering a distance of 922 km on the eastern continental margin of the UAE. The seismic reflections exhibit linear discontinuities representing fault surfaces. Several normal faults dissect the seismic profiles with minor displacements ranging from a few meters to a few tens of meters (Fig. 3a–d, f, g). Some of these faults

reach the seafloor (Fig. 3c, d), while others are deeply buried, i.e., blind faults (e.g., Fig. 3a, b). Several high-amplitude reflection anomalies or bright spots exist on the seismic profiles (Fig. 3a–d). A large area with polarity reversal is also noticed (Fig. 3e). The seismic data also show acoustic turbidity or seismic disturbances in several areas (Fig. 3a, d–g). There are depression-like features, i.e., pockmarks, at the top of some of the seismic profiles (e.g., Fig. 3a, d, e–g). However, other profiles do not show these features, but the bathymetric profiles show them as they are smaller than the seismic resolution (Fig. 3, insets 1 and 2). The acoustic turbidity areas are usually located
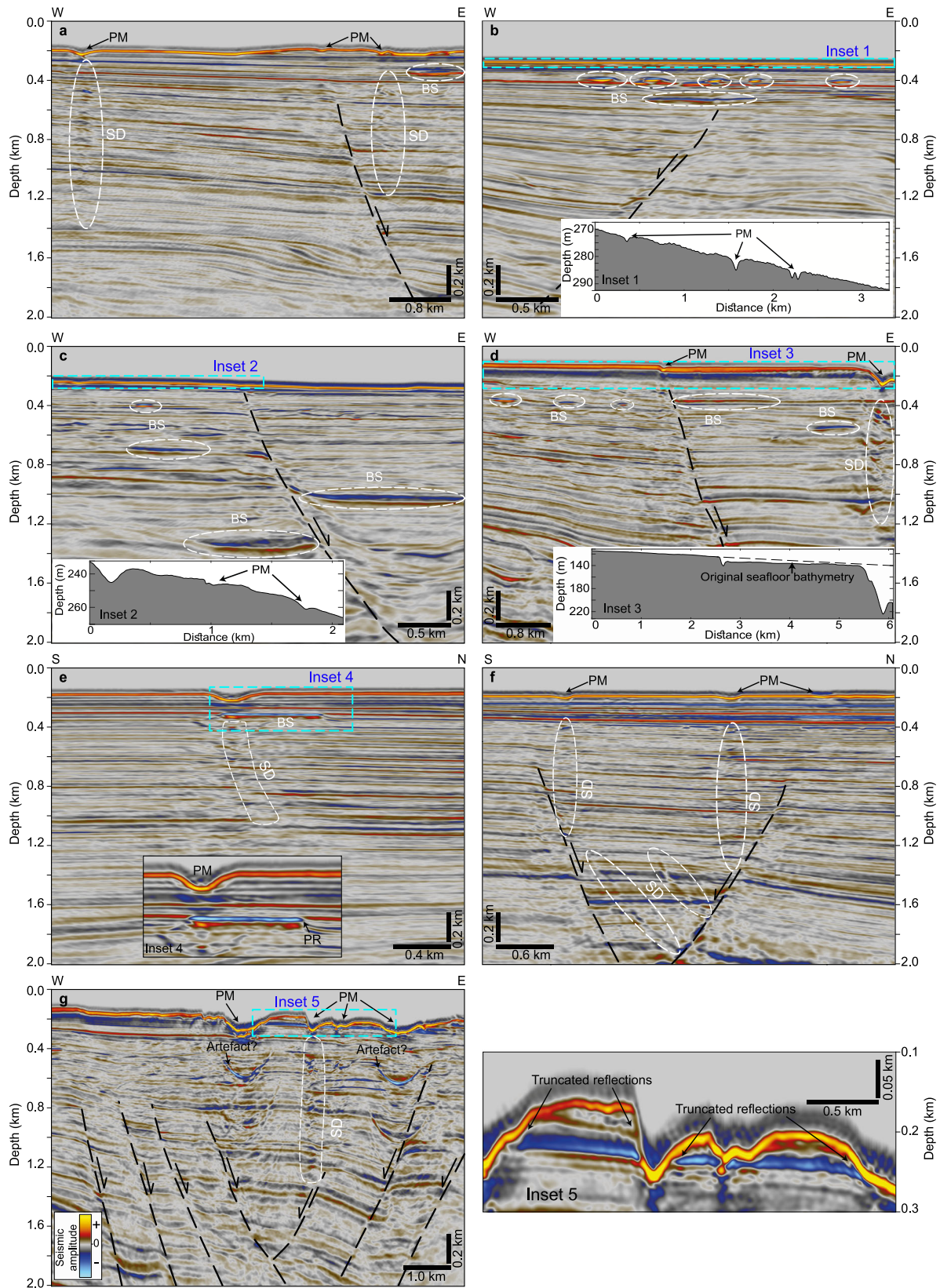
Fig. 3 | Seismic reflection profiles show how the pockmarks relate geometrically to the faults and the effect of erosion on the pockmark base. a A seismic profile illustrates the seismic disturbances (SD) or acoustic turbidity (that indicate fracture conduits), seafloor pockmarks, and fault conduits (black dashed line). **b, c** seismic profiles show several bright spots (BS), with insets 1 and 2 representing bathymetric profiles that show seafloor pockmarks across the same profiles. **d** Seismic profile shows the same features as **b, c**, in addition to inset 3, which illustrates the vertical displacement of the seafloor. **e** Inset 4 shows polarity reversal (PR). **f, g** Show several faults and fracture conduits below seafloor pockmarks, with inset 5 illustrating the erosional truncation of the seismic reflections by the seafloor.

Fig. 4 | Water column backscatter data (echograms) with the discovered gas seeps in the Gulf of Oman. a An echogram from the wideband echosounder data (at 18 kHz) showing evidence of fluid escaping from the seafloor, gas bubbles, over almost flat bathymetry. **b** An echogram showing several gas seeps over rugged bathymetry.
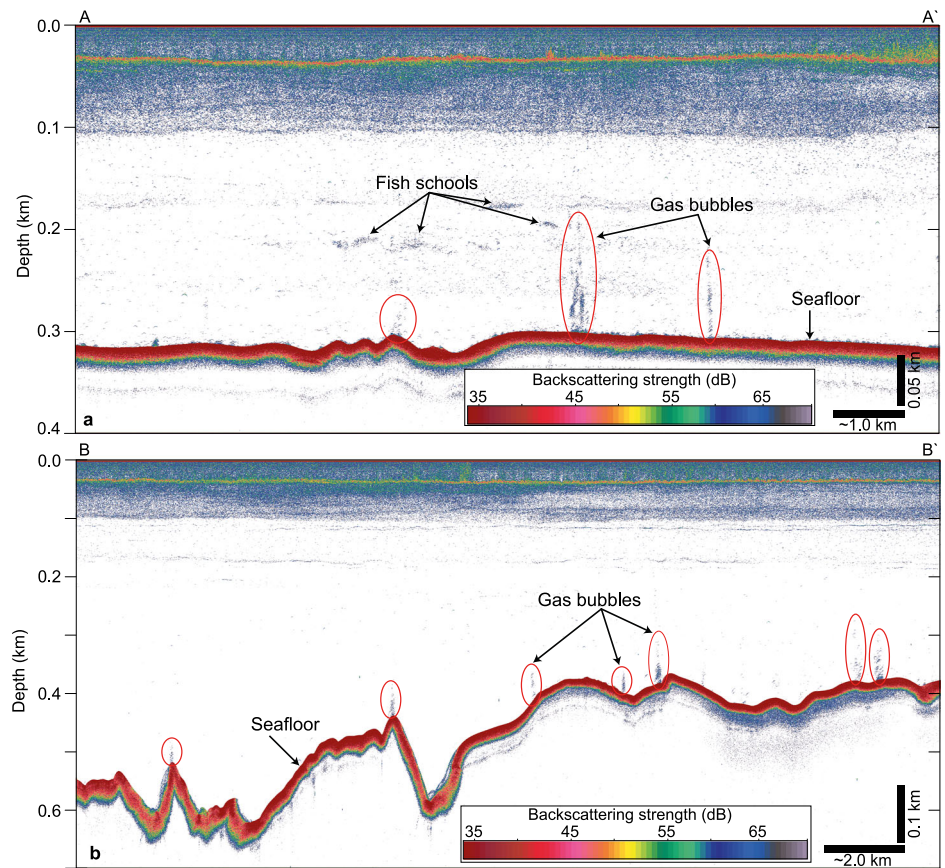
below the pockmarks (e.g., Fig. 3a western sector, 3d eastern sector, and 3e middle sector). Similarly, the pockmarks are located above normal faults (e.g., Fig. 3b–d middle sectors and Fig. 3g). In some areas, there are several truncations of the seismic reflections by the seafloor (Fig. 3, inset 5).

The backscatter of the water column from wideband echosounder data (Echograms) shows the seafloor as having very high-backscattering strength (Fig. 4). There are also columnar features above the seafloor (Fig. 4), exhibiting higher backscattering strength than the surrounding water body. They are extended from <50 m to >100 m above the seafloor. A total of 35 locations of these columnar high-backscattering features have been identified, occurring at 236-538 m water depths and mostly over flat areas (Fig. 4 and Supplementary Fig. 1).

Physical parameters of the water column

Profiles of the physical parameters of the water column (salinity, temperature, and beam attenuation) exhibit vertical layering along the UAE's eastern margin (Fig. 5). The profiles show three main water column layers. The shallow layer has a salinity of 37 PSU (Practical Salinity Unit), a temperature of 28 °C, and a beam attenuation coefficient of 0.25–0.36 m^{-1}. On the other hand, the second (middle) layer has low salinity, temperature, and beam attenuation of 36.25 PSU, 21–22 °C, and 0.1 m^{-1}, respectively. The deepest layer has high salinity, temperature, and beam attenuation of 38–39 PSU, 25–28 °C, and 0.25–0.36 m^{-1}, respectively (Fig. 5a–c). The deep layer thickness is about 25 m over the gently SE-sloping shelf bathymetry (Fig. 5a, b (between PPP 3 and 4)). However, when reaching the northern edge of the pockmark areas, this layer thickness increases up to 98 m (average of 64 m) (Fig. 5b at PPP 4). The depth limit of the seafloor where this layer detaches from the seafloor is around 230 m (see the bathymetry and PPPs in Fig. 5b between PPP 4 and 5, as well as Fig. 5c between PPP 8 and 9). The deep layer is extended to ~20–30 km after detaching from the seafloor (Fig. 5b between PPP 4 and 14, and Fig. 5c between PPP 8 and 14).

Discussion

The pockmarks are widespread across the UAE's eastern continental margin and limited to the shelf break; no pockmarks occur oceanward from the shelf break (Fig. 2a). Similar features were reported in the northwestern Arabian/Persian Gulf and the Strait of Hormuz at depths <100 m[3,45]. These pockmarks of the northwestern Arabian/Persian Gulf and the Strait of Hormuz were associated with thermogenic gas release[3,45]. However, these pockmarks are wider and shallower, which might be related to lithological differences[46].

All the observed pockmarks occur within an area that is curved but mainly oriented NE-SW (Fig. 2a). This trend is likely linked to a major normal gravitational fault, i.e., gravitational collapse with an inclined plane, occurring south of the study area (Fig. 1 inset). Levell et al.[36] initially identified the fault on seismic reflection data in the Sohar basin, located south of our study area. We hereby designate this fault as the Batinah Offshore Normal Fault (BOFNF). The fault reaches the seafloor, creating escarpment relief of ~245 m at its southern limits (based on regional bathymetry, Fig. 1, inset). The escarpment relief decreases to the north, reaching around 160 m in the middle portion of the fault to 30 m at its northern limit (southern edge of our area). The curved trend of the pockmark field possibly represents a damage zone as a northern extension of the BOFNF. This damage zone contains extensive normal faults with minor displacements and fractures (acoustic turbidity). In some areas, the fault displacement extends to the seafloor, creating a vertical seabed relief (e.g., 24 m vertical relief above the fault in Fig. 3d and inset 3). The damage zone structures acted as conduits for the gas, allowing it to escape from deeper to shallower levels, followed by further escape through the seafloor and the formation of pockmarks. Observing the regional trend of the BOFNF, this regional gravitational fault might represent a nucleation for a new shelf break in the mouth of the Strait of Hormuz. Further sediment loading on the hanging wall of the BOFNF may trigger more slip across the fault, generating earthquakes and forming a new shelf break in the Gulf of Oman.
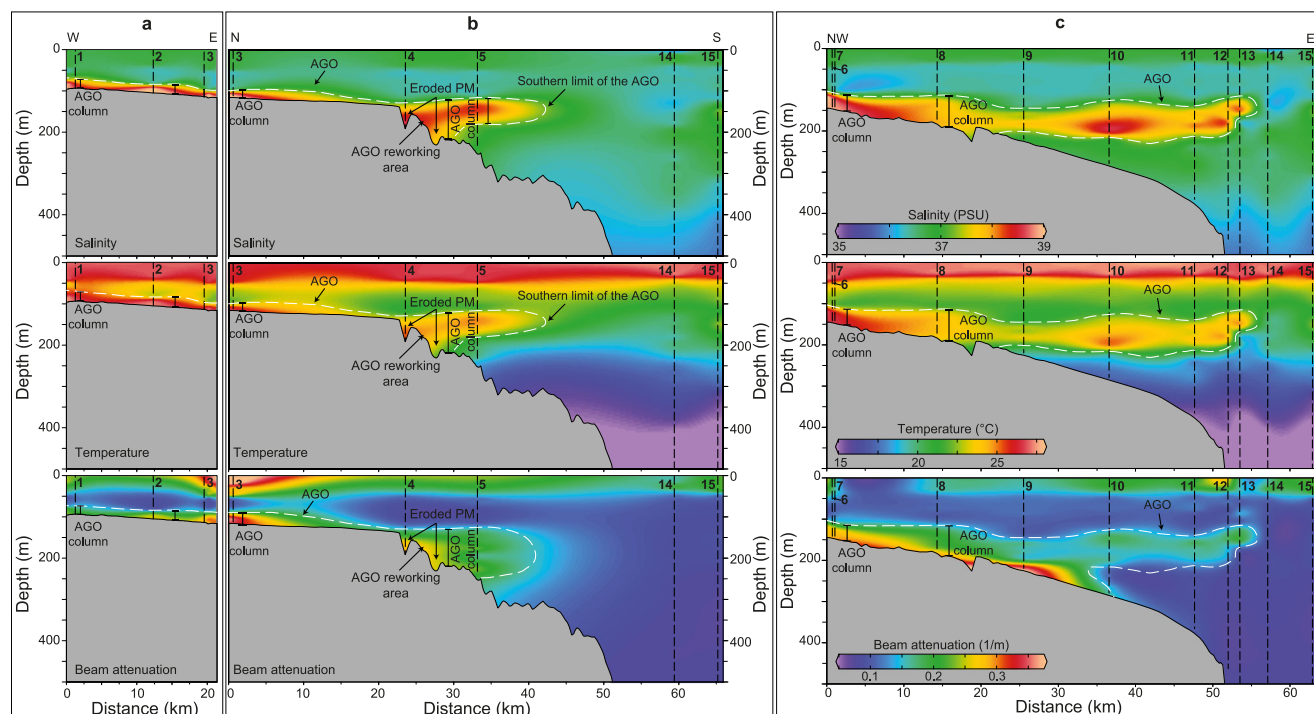
Fig. 5 | Sections of the water column physical parameters of the eastern offshore of the UAE. a An E-W section of the water column physical parameters showing the bottom Arabian Gulf Outflow (AGO), exhibiting mainly a uniform thickness over flat shelf bathymetry. The AGO is characterized by high salinity, temperature, and beam attenuation. **b, c** represent mainly N-S and E-W water column physical parameters sections, respectively, where the AGO has an almost uniform thickness over flat shelf bathymetry and exhibits reworking or generation of secondary currents, hence increased thickness, within the seafloor irregularities, i.e., pockmarks.

Several shallow bright spots, polarity reversal, and acoustic turbidity are identified on the seismic reflection profiles (Fig. 3). These seismic features represent evidence for subsurface gas accumulations in shallow levels. Shallow bright spots with reversed polarity in the seismic data usually suggest shallow gas accumulations[51–53]. Enhanced reflections exhibit high amplitude or reflectivity due to gas or fluid content in shallow sediments, and it is also called gas brightening or bright spots[3]. The studied shallow part of the sedimentary section is dissected by numerous normal faults, especially below the mapped pockmarks. This part also has acoustic turbidity in some areas that may be related to fracture conduits and gas escape (Fig. 3a, d–g). In seismic reflection data, acoustic turbidity, or gas chimneys, usually indicates uprising gases in the subsurface layers[54–56].

The columnar high-backscattering features identified on the water column backscatter data are interpreted as gas bubbles/seeps coming out of the seafloor. Several of these features occur within pockmarks (Fig. 2a). However, most are located on un-pockmarked seafloor; likely, over time, with increased or higher volumes of gas escape, these areas may become pockmarked. The gas accumulated in the shallower parts of the sedimentary section possibly migrated from the deeper levels across the normal faults and fracture conduits. A recent study conducted on the Fujairah basin by Abdelmaksoud and Ali[30] indicated that the area has an active petroleum system. They stated that most of the source rocks are gas-prone, and the gas maturation window has been reached within the sub-basins. They also identified several low-velocity anomalies that might indicate the occurrence of hydrocarbon accumulations. Biogenic origin for the escaping gas may also be considered. The Biogenic origin is supported by the high subsidence rate of the area in the last few million years[30], and hence the rapid burial and preservation of organic matter. The origin of the escaping gases might also be a mixed source of biogenic and thermogenic gases. However, sampling and analysis of the escaping gases are required to determine their exact origin.

Interestingly, there are conduits or evidence of gas accumulations below most of the identified seafloor pockmarks (Fig. 3). Consequently, a direct relationship exists between the pockmarks, subsurface conduits, and

gas accumulations. Some of the conduits reach the seafloor or just below it (Fig. 3c, d). However, other conduits do not reach the seafloor but possibly deliver gas to the shallower levels (e.g., Fig. 3a, b, f). Some of the trapped shallow gas accumulations are probably stationary (Fig. 3a, b, f, g). The trapped gases would remain so until enough gas builds up for the pressure to cause a break through the sealing layer[57]. A similar situation was found in the Norwegian Trench, where very shallow gas blankets have holes immediately below most of the pockmarks. It was indicated that the gas below the pockmarks has probably migrated up through them[57]. Similarly, shallow gas accumulations (and gas chimneys) were correlated with seafloor gas escaping features in the western offshore areas of the Egyptian Nile Delta[54]. However, consistent with previous observations[1,58], pockmarks are not spatially correlated with active gas seeps.

Another interesting feature of the pockmark field is the arrangement in a curved trend, occurring parallel to the shelf break (Fig. 2a). The presence of pockmark strings and elongated and eroded pockmarks characterize the northern limit of the pockmarks. Moving towards the shelf break, considering the curved trend, the next area is characterized mainly by circular pockmarks (Fig. 2a), with less or no impact of erosion, indicated by the uniform circular shapes of these features. The discovered gas seeps in this study are located shelf-ward from these pockmark areas. This succession of occurrence of pockmarks and gas seeps possibly indicates that the northern pockmark field represents the oldest gas seeps that are likely no longer active and had sufficient time to enlarge, followed by the second area with the circular or unit pockmarks, which is followed by the active gas leakage area which we assume will be pockmarked in the future after releasing sufficient volumes of gas (Fig. 2a).

The deep-water layer identified on the sections of the PPPs of the water column (Fig. 5) is interpreted as a deep flow of the Arabian/Persian Gulf (here, referred to as the Arabian Gulf Outflow, AGO). The AGO has higher salinity, water temperature, and beam attenuation than the overlying water column, with nearly similar physical characteristics to the surface water layer. Arabian Gulf water is known for its high salinity and temperature[59]. This water stratification has also previously been reported in the Strait of Hormuz[60–63].

In the northernmost area of mapping (Figs. 1 and 2a), several pockmarks are elongated, and many crescent-shaped pockmarks are also interconnected, indicating the possible effect of erosion. The crescent-shaped pockmarks result from the erosion by currents of the circular pockmarks[64,65]. Additionally, the seismic sections crossing some of the pockmarks show evidence of erosion with truncation of seismic reflections by the pockmark walls, where the uppermost sediment layer is absent, and the older ones are exposed within the trough of these features (Fig. 3g inset 5). The presence of several pockmark strings (connected pockmarks, Fig. 2a, c, d) indicates the effect of currents and erosion in removing the sediment between pockmarks to create an interconnected string of pockmarks. Many pockmark strings end in a single pockmark much larger than those forming the string[3].

The increase in the AGO thickness at the northern edge of the pockmark field indicates the turbulence or reworking of the AGO current caused by the seafloor obstacles or irregularities, i.e., pockmarks and slight seabed vertical relief (Fig. 3d middle sector, 5b at PPP 4). These irregularities led to steeper slope gradients and subsequently increased the AGO current velocities, generating secondary erosional currents or large eddies. Large eddies were suggested to be formed due to seafloor bathymetry changes in the Strait of Hormuz channel[66]. The AGO secondary currents are likely responsible for the erosion of the relatively deeper areas represented by the pockmarks. The high beam attenuation of the bottom water layer within the pockmark strings (Fig. 5a–c) possibly indicates the higher turbidity within the troughs of these features and, hence, the effect of the AGO current turbulence. Generally, along the regional current pathway, the seafloor irregularities modify the velocity; the higher the slope gradient, the higher the velocity[67,68]. A scarcity of late Holocene deposits near the Musandam Peninsula and the Strait of Hormuz is attributed to erosion by the bottom water exiting the Arabian/Persian Gulf via the Strait of Hormuz[46].

On the continental shelf, the AGO is extended farther south across the Omani margin[60,63]. This may indicate fewer seafloor irregularities or obstacles that could prevent the outflow from traveling farther south across the smooth continental shelf. On the other hand, around the pockmark field, the secondary/reworked AGO currents are then detached from the seafloor and extended through an intermediate depth layer of the water column to around 20 to 30 km southward of the northern limit of the pockmarks within the deep Gulf of Oman water. The AGO possibly has a very low negative buoyancy over the continental shelf area, allowing it to flow over the seabed. However, the detaching of the AGO from the seabed southward of the northern limit of the pockmark field indicates the effect of water mixing within the pockmarks and increasing the buoyancy of the AGO, i.e., reaching neutral buoyancy. This neutral buoyancy allows the AGO to flow at an intermediate water level.

Based on this study, the pockmark occurrence is restricted to the seafloor, and there are no pockmarks identified in the shallow subsurface sedimentary sequence up to 2 km depth below the seafloor on the seismic sections (Fig. 3). This observation, together with the active gas seeps, indicates that the pockmark field possibly started ejecting gas into the Gulf of Oman water <14 thousand years ago after the deposition of the surface sediments. Owens et al.[47] reported high surface water methane concentrations and fluxes to the atmosphere in the Arabian Sea, including the Gulf of Oman. They stated that methane production is associated with high phytoplankton biomass and monsoon-driven upwelling of nutrient-rich water. The Arabian Sea represents only 0.43% of the total surface area of the oceans[47], however, Owens et al.[47] noted that it can contribute >1.3% of the total oceanic flux of methane. Therefore, they added that the current oceanic flux should be revised upwards, and other potential oceanic sources should be evaluated. The high methane concentrations in their maps correlate with the northern part of the Gulf of Oman (our study area), where we found the pockmarks and gas seeps. The active seafloor seeps may contribute additional methane to the atmosphere. Since the area is a low-oxygen continental margin[69], this may allow the escaped gases from the seafloor to continue to the atmosphere; if these gases are mainly methane. The low-oxygen concentrations and shallower water conditions in the Gulf of Oman will slow the oxidation process likely resulting in methane venting to the atmosphere increasing greenhouse gas flux out of

the sea in this area. However, further research is needed to understand the volume of gas accumulated in the subsurface on the UAE-Oman continental margin and how much is seeping and reaching the atmosphere to improve our flux estimates to the atmosphere.

Methods

Seismic data and interpretation
A marine geophysical dataset was acquired in the eastern offshore region of Fujairah and Sharjah emirates of the UAE using SeaBird Exploration's M/V Hawk Explorer in July 2014, under the sponsorship of the Petroleum Institute, now known as Khalifa University. The seismic dataset comprises 20 2D reflection profiles in the depth domain with a positive increase in acoustic impedance represented as red. The total length of the seismic profiles is 922 km. Petrel^{TM} Schlumberger software was used to visualize and analyze the seismic data and interpret the structural features/conduits and the bright spots. Faults were visually identified by the displacement of seismic reflections, where acoustic turbidity was used as a possible indication of fracture conduits. The high-amplitude reflections in a low-amplitude background were used to indicate gas accumulations.

Multibeam bathymetry
The high-resolution multibeam bathymetry was acquired using the OceanXplorer vessel (owned by OceanX) in December 2023. The data were acquired with an average speed of 7.5 knots (kn). Kongsberg^{TM} EM712 echosounder with Kongsberg^{TM} Seafloor Information System (SIS) was used for data acquisition, whereas Qimera QPS^{TM} software was used for data processing onboard the OceanXplorer vessel. Qimera was also used for 2D and 3D data visualizations. Bathymetric profile data were extracted from Qimera and plotted. The slope gradient and curvature were calculated for the bathymetry data using ArcMap ESRI^{TM}.

Water column backscatter
The water column backscatter data (wideband echosounder data) were acquired using the Kongsberg^{TM} Simrad EK80 split-beam echosounder of the OceanXplorer vessel in December 2023. The system uses a wide range of frequencies (18, 38, 70, 120, 200, and 333 kHz). The processed data were replayed and visualized in Echoview^{TM} software. The gas bubbles were more apparent on the 18 kHz display; therefore, this frequency was used to detect the gas bubbles across the entire dataset. The gas bubbles were identified by their higher backscattering volume strength than the surrounding water and distinguishable columnar shapes/plumes originating from the seafloor.

Water column PPPs
PPPs of the water were measured using OceanXplorer CTD Rosette, which includes a multi-channel logger capable of measuring temperature, salinity, and beam attenuation throughout the water column. Fifteen PPPs/CTDs were acquired and used in this study. The temperature, salinity, and beam attenuation were plotted as 2D sections using Ocean Data View (ODV) software[70]. The sections were then used to interpret the water stratification and distribution of the different PPPs and their implications.

Reporting summary
Further information on research design is available in the Nature Portfolio Reporting Summary linked to this article.

Data availability
Multibeam bathymetry, water column PPPs and backscatter, and seismic reflection data are available at [https://doi.org/10.6084/m9.figshare.28068422]. The regional topography/bathymetry dataset is publicly available (GEBCO grid 2024[71]) at [https://download.gebco.net/].

References

1. Hovland, M., Gardner, J. V. & Judd, A. The significance of pockmarks to understanding fluid flow processes and geohazards. *Geofluids* **2**, 127–136 (2002).
2. Hovland, M.& Judd, A. G. Seabed pockmarks and seepages: impact on geology, biology and the marine environment. Graham & Trotman London (1988).
3. Judd, A., Hovland, M. Seabed fluid flow: the impact on geology, biology and the marine environment. Cambridge University Press (2009).
4. Brothers, L. L. et al. Shallow stratigraphic control on pockmark distribution in north temperate estuaries. *Mar. Geol.* **329**, 34–45 (2012).
5. Chen, S. et al. Anomalous depressions in the northern Yellow Sea Basin: evidences for their evolution processes. *Mar. Pet. Geol.* **84**, 179–194 (2017).
6. Andreassen, K. et al. Massive blow-out craters formed by hydrate-controlled methane expulsion from the Arctic seafloor. *Science* **356**, 948–953 (2017).
7. Sultan, N. et al. Pockmark formation and evolution in deep water Nigeria: rapid hydrate growth versus slow hydrate dissolution. *J. Geophys. Res. Solid Earth* **119**, 2679–2694 (2014).
8. Ruffine, L. et al. Investigation on the geochemical dynamics of a hydrate-bearing pockmark in the Niger Delta. *Mar. Pet. Geol.* **43**, 297–309 (2013).
9. Shakhova, N. et al. Current rates and mechanisms of subsea permafrost degradation in the East Siberian Arctic Shelf. *Nat. Commun.* **8**, 15872 (2017).
10. Andresen, K. J. & Huuse, M. 'Bulls-eye' pockmarks and polygonal faulting in the Lower Congo Basin: relative timing and implications for fluid expulsion during shallow burial. *Mar. Geol.* **279**, 111–127 (2011).
11. Chenrai, P. & Huuse, M. Pockmark formation by porewater expulsion during rapid progradation in the offshore Taranaki Basin, New Zealand. *Mar. Pet. Geol.* **82**, 399–413 (2017).
12. Hübscher, C. & Borowski, C. Seismic evidence for fluid escape from Mesozoic cuesta type topography in the Skagerrak. *Mar. Pet. Geol.* **23**, 17–28 (2006).
13. Jensen, J. B., Kuijpers, A., Bennike, O., Laier, T. & Werner, F. New geological aspects for freshwater seepage and formation in Eckernförde Bay, western Baltic. *Continent. Shelf Res.* **22**, 2159–2173 (2002).
14. Reusch, A. et al. Giant lacustrine pockmarks with subaqueous groundwater discharge and subsurface sediment mobilization. *Geophys. Res. Lett.* **42**, 3465–3473 (2015).
15. Davy, B., Pecher, I., Wood R., Carter L.& Gohl K. Gas escape features off New Zealand: evidence of massive release of methane from hydrates. *Geophys. Res. Lett.* **37** (2010).
16. Ingrassia, M. et al. The Zannone Giant Pockmark: first evidence of a giant complex seeping structure in shallow-water, central Mediterranean Sea, Italy. *Mar. Geol.* **363**, 38–51 (2015).
17. Riboulot, V., Sultan, N., Imbert, P. & Ker, S. Initiation of gas-hydrate pockmark in deep-water Nigeria: geo-mechanical analysis and modelling. *Earth Planet. Sci. Lett.* **434**, 252–263 (2016).
18. Wenau, S., Spieß, V., Pape, T. & Fekete, N. Controlling mechanisms of giant deep water pockmarks in the Lower Congo Basin. *Mar. Pet. Geol.* **83**, 140–157 (2017).
19. Chen, J. et al. Morphologies, classification and genesis of pockmarks, mud volcanoes and associated fluid escape features in the northern Zhongjiannan Basin, South China Sea. *Deep Sea Res. Part II: Top. Stud. Oceanogr.* **122**, 106–117 (2015).
20. Hillman, J. I., Gorman, A. R. & Pecher, I. A. Geostatistical analysis of seafloor depressions on the southeast margin of New Zealand's South Island—Investigating the impact of dynamic near seafloor processes on geomorphology. *Mar. Geol.* **360**, 70–83 (2015).
21. Hillman, J. I. et al. The diverse morphology of pockmarks around Aotearoa New Zealand. *Front. Mar. Sci.* **10**, 1235928 (2023).
22. Schattner, U., Lazar, M., Souza, L., Ten Brink, U. & Mahiques MMd. Pockmark asymmetry and seafloor currents in the Santos Basin offshore Brazil. *Geo-Mar. Lett.* **36**, 457–464 (2016).
23. García, M. et al. Erosive sub-circular depressions on the Guadalquivir Bank (Gulf of Cadiz): interaction between bottom current, mass-wasting and tectonic processes. *Mar. Geol.* **378**, 5–19 (2016).
24. Hillman, J. I. et al. Gas migration pathways and slope failures in the Danube Fan, Black Sea. *Mar. Pet. Geol.* **92**, 1069–1084 (2018).
25. Isola, J. I. et al. The late-quaternary deposits of the Piedra Buena Terrace (Patagonian continental slope, SW Atlantic): an example of interaction between bottom currents and seafloor morphology. *Mar. Geol.* **435**, 106459 (2021).
26. Klaucke, I. et al. Giant depressions on the Chatham Rise offshore New Zealand–morphology, structure and possible relation to fluid expulsion and bottom currents. *Mar. Geol.* **399**, 158–169 (2018).
27. Micallef, A. et al. Multiple drivers and controls of pockmark formation across the Canterbury Margin, New Zealand. *Basin Res.* **34**, 1374–1399 (2022).
28. Miramontes, E. et al. Contourite distribution and bottom currents in the NW Mediterranean Sea: coupling seafloor geomorphology and hydrodynamic modelling. *Geomorphology* **333**, 43–60 (2019).
29. Warnke, F. et al. Evolution of complex giant seafloor depressions at the northern Argentine continental margin (SW Atlantic Ocean) under the influence of a dynamic bottom current regime. *Front. Earth Sci.* **11**, 1117013 (2023).
30. Abdelmaksoud, A. & Ali, M. Y. Petroleum system analysis of Fujairah basin, eastern offshore of the United Arab Emirates. *Mar. Pet. Geol.* **170**, 107157 (2024).
31. Mokhtari, M., Abdollahie Fard, I. & Hessami, K. Structural elements of the Makran region, Oman sea and their potential relevance to tsunamigenisis. *Nat. Hazards* **47**, 185–199 (2008).
32. White, R. & Klitgord, K. Sediment deformation and plate tectonics in the Gulf of Oman. *Earth Planet. Sci. Lett.* **32**, 199–209 (1976).
33. White, R. S. Active and passive plate boundaries around the Gulf of Oman, north-west Indian Ocean. *Deep Sea Res. Part A Oceanogr. Res. Pap.* **31**, 731–745 (1984).
34. White, R. S. & Ross, D. A. Tectonics of the western Gulf of Oman. *J. Geophys. Res. Solid Earth* **84**, 3479–3489 (1979).
35. Ali, M. et al. Geophysical imaging of ophiolite structure in the United Arab Emirates. *Nat. Commun.* **11**, 1–10 (2020).
36. Levell, B. et al. Geological and seismic evidence for the tectonic evolution of the NE Oman continental margin and Gulf of Oman. *Geosphere* **17**, 1472–1493 (2021).
37. Ravaut, P., Bayer, R., Hassani, R. & Rousset, D. Al Yahya'ey A. Structure and evolution of the northern Oman margin: gravity and seismic constraints over the Zagros-Makran-Oman collision zone. *Tectonophysics* **279**, 253–280 (1997).
38. Styles M. et al. The geology and geophysics of the United Arab Emirates. *Geology* **2** (2006).
39. Thurley, C. et al. Tectonostratigraphic evolution of the Sohar Basin, exploration concepts and emerging plays offshore on the UAE's east coast. *Mar. Pet. Geol.* **143**, 105807 (2022).
40. Abdelmaksoud, A., Ali, M., Geng, M. & Saibi, H. Basement morphology of the fold-and-thrust belt and foreland basin of the United Arab Emirates: evidence for thick-skinned tectonics in the northern Oman-UAE Mountains. *Tectonophysics* **856**, 229838 (2023).
41. Abdelmaksoud, A., Ali, M. & Searle, M. Tectono-stratigraphic evolution of the foreland fold-and-thrust belt of the United Arab Emirates. *Tectonics* **41**, e2022TC007470 (2022).
42. Searle M. Geology of the Oman mountains, Eastern Arabia. Springer (2019).

43. Stoffers, P. & Ross, D. A. Late Pleistocene and Holocene sedimentation in the Persian Gulf—Gulf of Oman. *Sediment. Geol.* **23**, 181–208 (1979).

44. Hosseinyar, G., Moussavi-Harami, R. & Behbahani, R. Shallow gas accumulations and seepage in the sediments of the Northeast Persian Gulf. *Acta Geophys.* **62**, 1373–1386 (2014).

45. Ellis, J. P. & McGuinness, W. T. Pockmarks of the northwestern Arabian Gulf. In: *Oceanology: Proceedings of an international conference (Oceanology International'86), sponsored by the Society for Underwater Technology, and held in Brighton, UK*, 4–7). Springer (1986).

46. Uchupi, E., Swift, S. & Ross, D. Gas venting and late quaternary sedimentation in the Persian (Arabian) Gulf. *Mar. Geol.* **129**, 237–269 (1996).

47. Owens, N., Law, C., Mantoura, R., Burkill, P. & Llewellyn, C. Methane flux to the atmosphere from the Arabian Sea. *Nature* **354**, 293–296 (1991).

48. Lachkar, Z., Levy, M., Hailegeorgis, D. & Vallivattathillam, P. Differences in recent and future trends in the Arabian Sea oxygen minimum zone: processes and uncertainties. *Front. Mar. Sci.* **10**, 1122043 (2023).

49. Arya, K. et al. Distribution and sea-to-air fluxes of nitrous oxide and methane from a seasonally hypoxic coastal zone in the southeastern Arabian Sea. *Mar. Pollut. Bull.* **205**, 116614 (2024).

50. Naqvi, S. W. A. et al. Biogeochemical ocean-atmosphere transfers in the Arabian Sea. *Prog. Oceanogr.* **65**, 116–144 (2005).

51. Ferré, B. et al. Reduced methane seepage from Arctic sediments during cold bottom-water conditions. *Nat. Geosci.* **13**, 144–148 (2020).

52. Fischer, D. et al. Subduction zone earthquake as potential trigger of submarine hydrocarbon seepage. *Nat. Geosci.* **6**, 647–651 (2013).

53. Sarkar S. et al. Seismic evidence for shallow gas-escape features associated with a retreating gas hydrate zone offshore west Svalbard. *J. Geophys. Res. Solid Earth* **117** (2012).

54. Ismail, A. et al. The detection of deep seafloor pockmarks, gas chimneys, and associated features with seafloor seeps using seismic attributes in the West offshore Nile Delta, Egypt. *Explor. Geophys.* **52**, 388–408 (2021).

55. Ismail, A., Ewida, H. F., Nazeri, S., Al-Ibiary, M. G. & Zollo, A. Gas channels and chimneys prediction using artificial neural networks and multi-seismic attributes, offshore West Nile Delta, Egypt. *J. Pet. Sci. Eng.* **208**, 109349 (2022).

56. Ismail, A., Radwan, A. A., Leila, M. & Eysa, E. A. Integrating 3D subsurface imaging, seismic attributes, and wireline logging analyses: implications for a high resolution detection of deep-rooted gas escape features, eastern offshore Nile Delta, Egypt. *J. Afr. Earth Sci.* **213**, 105230 (2024).

57. Hovland, M. Elongated depressions associated with pockmarks in the western slope of the Norwegian trench. *Mar. Geol.* **51**, 35–46 (1983).

58. Skarke, A., Ruppel, C., Kodis, M., Brothers, D. & Lobecker, E. Widespread methane leakage from the sea floor on the northern US Atlantic margin. *Nat. Geosci.* **7**, 657–661 (2014).

59. Thompson, E. F.& Gilson, H. C. Chemical and physical investigations: introduction. AbeBooks (1937).

60. Bidokhti, A. & Ezam, M. The structure of the Persian Gulf outflow subjected to density variations. *Ocean Sci.* **5**, 1–12 (2009).

61. Ghazi, E., Bidokhti, A. A., Ezam, M., Azad, M. T. & Hassanzadeh, S. Physical properties of Persian Gulf outflow thermohaline intrusion in the Oman Sea. *Open J. Mar. Sci.* **7**, 169–190 (2016).

62. Kämpf, J. & Sadrinasab, M. The circulation of the Persian Gulf: a numerical study. *Ocean Sci.* **2**, 27–41 (2006).

63. Bower, A. S., Hunt, H. D. & Price, J. F. Character and dynamics of the Red Sea and Persian Gulf outflows. *J. Geophys. Res.: Oceans* **105**, 6387–6414 (2000).

64. Cukur, D. et al. Morphology and genesis of giant seafloor depressions on the southeastern continental shelf of the Korean Peninsula. *Mar. Geol.* **415**, 105966 (2019).

65. Josenhans, H. W., King, L. H. & Fader, G. B. A side-scan sonar mosaic of pockmarks on the Scotian Shelf. *Can. J. Earth Sci.* **15**, 831–840 (1978).

66. Swift, S. A. & Bower, A. S. Formation and circulation of dense water in the Persian/Arabian Gulf. *J. Geophys. Res. Oceans* **108**, 4-1–4-21 (2003).

67. Faugères J.-C. & Mulder T. Contour currents and contourite drifts. *Dev. Sedimentol.* **63**, 149–214 (2011).

68. Hillman, J. I. et al. The influence of submarine currents associated with the Subtropical Front upon seafloor depression morphologies on the eastern passive margin of South Island, New Zealand. *N.Z. J. Geol. Geophys.* **61**, 112–125 (2018).

69. Queste, B. Y., Vic, C., Heywood, K. J. & Piontkovski, S. A. Physical controls on oxygen distribution and denitrification potential in the North West Arabian Sea. *Geophys. Res. Lett.* **45**, 4143–4152 (2018).

70. Schlitzer R. Ocean data view https://odv.awi.de. (2024).

71. Kapoor, D. General bathymetric chart of the oceans (GEBCO). *Mar. Geod.* **5**, 73–80 (1981).

Acknowledgements

Author contributions

A.A., A.H.A., and M.Y.A. designed the study. A.A., M.A., A.S., S.A., and L.A. collected the marine data onboard OceanXplorer. M.Y.A. collected the seismic data onboard Hawk Explorer. A.A. performed the formal analysis, generated the figures, and wrote the original draft. A.H.A and M.Y.A. obtained the funding, validated the results, and reviewed the manuscript. All authors read and approved the final manuscript.

Competing interests

The authors declare no competing interests.

Additional information

Supplementary information The online version contains supplementary material available at https://doi.org/10.1038/s43247-025-02009-6.

Correspondence and requests for materials should be addressed to Ahmed Abdelmaksoud.

Peer review information *Communications earth and environment* thanks Amir Ismail, Boda Zhang and Neil Mitchell for their contribution to the peer review of this work. Primary Handling Editors: Alice Drinkwater. A peer review file is available.

Reprints and permissions information is available at http://www.nature.com/reprints

Publisher's note Springer Nature remains neutral with regard to jurisdictional claims in published maps and institutional affiliations.